Available online at www.sciencedirect.com
ScienceDirect
Journal of Sound and Vibration 300 (2007) 1–12
JOURNAL OF SOUND AND VIBRATION
www.elsevier.com/locate/jsvi

Engine noise potential analysis for a trimmed vehicle body: Optimisation using an analytical sea gradient computation technique

Thorsten Bartosch*, Tamino Eggner

MAGNA STEYR Fahrzeugtechnik AG & Co KG, Department of Vehicle Acoustics, Liebenauer Hauptstrasse 317, 8041 Graz, Austria

Received 14 November 2005; received in revised form 11 May 2006; accepted 14 June 2006
Available online 29 September 2006

Abstract

For the optimisation of the vibro-acoustic behaviour of vehicle bodies above 400 Hz, statistical energy analysis (SEA) has become a common tool in recent years. Within this paper we would like to introduce a vibro-acoustic optimisation algorithm which is based on an analytical gradient computation of the energy of a subsystem with respect to SEA coupling and internal loss factors. The suggested interface of the method between vibro-acoustic complete vehicle optimisation with respect to SEA parameters and material optimisation in order to design the SEA loss factors, might offer a suitable work flow between OEM or system supplier and trim material supplier. With the help of the analytical gradient formulation, which is represented in Section 2, we show in Section 3 that the energy of subsystems, which constitutes the optimisation function, does not exhibit local extrema in the loss factor parameter space. Therefore, a straightforward optimisation procedure based on the investigation of the vibro-acoustic potentials of loss factors and the calculation of design targets is introduced in Section 4. After validation in Section 5 the method is applied in Section 6 in order to optimise engine noise of a coupé SEA model.

1. Introduction

Statistical Energy Analysis (SEA) was first introduced by Lyon and Maidanik [1] and Smith [2], but its application to vehicle body high-frequency vibro-acoustics is relatively recent. The SEA modelling technique exploits the fact, that for higher frequencies, a complex vibro-acoustic structure can be partitioned into so-called subsystems (plates, cavities, etc.) according to the spatial extension of local mode groups. The state variable energy of a subsystem is interpreted in a statistical sense (spatial and frequency band averaging), hence no phase information is available. For a detailed introduction to SEA theory see e.g. Ref. [3].

The steady-state SEA equation which computes the total average energy of subsystems is given by

$$\omega_m \mathbf{L}(\omega_m)\mathbf{E}(\omega_m) = \mathbf{P}(\omega_m), \tag{1}$$

*Corresponding author.
E-mail address: thorsten.bartosch@magnasteyr.com (T. Bartosch).

0022-460X/$ - see front matter © 2006 Elsevier Ltd. All rights reserved.
doi:10.1016/j.jsv.2006.06.069

where

$$\mathbf{L} = \begin{bmatrix} \eta_{11} + \sum_j \eta_{1j} & -\eta_{21} & \cdots \\ -\eta_{12} & \eta_{22} + \sum_j \eta_{2j} & \cdots \\ \vdots & & \ddots \\ -\eta_{1j} & \cdots & \eta_{jj} + \sum_j \eta_{ij} \end{bmatrix} \tag{2}$$

is the non-symmetric SEA matrix which consists of frequency-dependent coupling $\eta_{ij}(\omega_m) \geqslant 0,\ i,j,m \in \mathbf{N}, i \neq j$ (CLFs) and internal loss factors $\eta_{ii}(\omega_m) > 0$ (ILFs). Without loss of generality ω_m represents the angular centre frequency of a 1/3-octave frequency band, where m is the band number. The components E_i of the vector $\mathbf{E}$ describe the total average energies and the components P_i of the vector $\mathbf{P}$ are the input powers of the subsystems S_i. The CLFs are related by the consistency equation

$$\eta_{ij} n_i = \eta_{ji} n_j, \tag{3}$$

with the modal density $n_i = N_i/\Delta\omega_m$ of the subsystem S_i. N_i denotes the number of modes within the bandwidth $\Delta\omega_m$ of the 1/3-octave band ω_m.

Assuming that $\mathbf{L}$ is invertible, then solving Eq. (1) results in the vector of energies

$$\mathbf{E}(\omega_m) = \mathbf{f}(\omega_m, \boldsymbol{\eta}(\omega_m)), \tag{4}$$

where

$$\boldsymbol{\eta}(\omega_m) = [\eta_{11}, \eta_{12}, \ldots, \eta_{21}, \eta_{22}, \ldots, \eta_{ij}, \ldots, \eta_{KK}]^{\mathrm{T}} \tag{5}$$

is the vector of sorted loss factors of dimension $(1, K^2)$ with $i,j = 1(1)K$.

For vibro-acoustic optimisation usually the power flows between subsystems and dissipated powers, which are both computed out of the subsystem energies using $P_{ij}(\omega_m) = \omega_m \eta_{ij} E_i(\omega_m)$, are optimised according to the acoustic target settings of the OEM. In addition there are some approaches, e.g. Refs. [4–8] which use optimisation theory in oder to do vehicle trim optimisation.

The above-mentioned approaches have the disadvantage that there is no direct identification of sensitivities of the frequency-dependent vibro-acoustic paths with respect to SEA model parameters which would help to understand how an, e.g. in-cabin sound pressure level (SPL) at a certain frequency depends on SEA model parameters.

2. Sensitivity of loss factors

Therefore it seems very useful to investigate the gradient (sensitivity) of the energy in Eq. (4)

$$\mathbf{G}(\mathbf{E}, \omega_m) = \nabla_\eta \mathbf{E}^{\mathrm{T}}(\omega_m, \boldsymbol{\eta}(\omega_m)). \tag{6}$$

By neglecting Eq. (3) an efficient formula is derived in e.g. Ref. [9] which allows the numerical computation of the gradient. On the other hand these results reveal little about properties of the gradient. In Ref. [10] an analytical approach which is valid for small-energy variations around a given centre energy is given. In the following, we overcome this limitation and present the analytical structure of the gradient of the energy with respect a loss factor.

The set of loss factors η_{ij} can be interpreted as the parameter space $\boldsymbol{\eta} \in \mathbf{R}_+^{K^2}$. The auxiliary constraint (3) defines a sub-manifold within $\mathbf{R}^2$ that is related to the coordinates η_{ij} and η_{ji}. To avoid this linear dependency between basis vectors, all $\eta_{ij} \forall i > j$ in Eq. (2) are substituted using Eq. (3) which results in the matrix $\tilde{\mathbf{L}}$ and the energy $\tilde{\mathbf{E}}(\omega_m, \tilde{\boldsymbol{\eta}})$. Here $\{\tilde{\boldsymbol{\eta}} \in \mathbf{R}_+^{\tilde{K}} | \tilde{K} = K(K+1)/2\}$ means the reduced parameter space where all dimensions η_{ij} with $i > j$ are removed. Then, the del operator is defined as

$$\nabla_{\tilde{\eta}} = \left[\frac{\partial}{\partial \tilde{\eta}_{11}}, \frac{\partial}{\partial \tilde{\eta}_{12}}, \ldots, \frac{\partial}{\partial \tilde{\eta}_{ij}}, \ldots, \frac{\partial}{\partial \tilde{\eta}_{\tilde{K}\tilde{K}}} \right]^{\mathrm{T}} \quad \forall i \leqslant j. \tag{7}$$

After substituting Eq. (1) in Eq. (6) we get

$$\mathbf{G}(\tilde{\mathbf{E}}, \omega_m) = \frac{1}{\omega_m} \nabla_{\tilde{\eta}}((\tilde{\mathbf{L}}^{-1}(\omega_m)\mathbf{P}(\omega_m))^{\mathrm{T}}). \tag{8}$$

The column i of the matrix $\mathbf{G}$ is related to the sensitivities of the ith energy component of $\tilde{\mathbf{E}}$. Assuming a SEA model size of K subsystems, then $\tilde{\mathbf{E}}, \mathbf{P}$ have dimension K, and $\tilde{\mathbf{L}}$ is an (K, K) matrix. Furthermore, one can see that the gradient is strongly dependent on the source configuration of the model which is given by the vector $\mathbf{P}$.

A direct analytical solution of Eq. (8) rapidly becomes too involved when the model size increases to the usual subsystem count of approximately 100 to 500, which is easily reached for vehicle simulations.

For simplicity we restrict ourselves to the component $\tilde{E}_i$. Therefore Eq. (8) becomes the vector

$$\mathbf{G}^i(\tilde{E}_i, \omega_m) = \frac{1}{\omega_m} (\nabla_{\tilde{\eta}}((\tilde{\mathbf{L}}^{-1}(\omega_m)\mathbf{P}(\omega_m))^{\mathrm{T}}))\mathbf{e}_i, \tag{9}$$

with the ith unit vector $\mathbf{e}_i$ of dimension K. When considering only the component $G^i_{sl}(\tilde{E}_i, \omega_m)$ we have, with $x = \tilde{\eta}_{sl}$

$$G^i_{sl}(\tilde{E}_i, \omega_m) = G^i_{sl}(\tilde{\boldsymbol{\eta}}(x), \omega_m) = \frac{1}{\omega_m} \frac{\partial}{\partial x} ((\tilde{\mathbf{L}_{sl}}^{-1}(x)\mathbf{P}) \cdot \mathbf{e}_i). \tag{10}$$

The gradient calculation in Eq. (10) can be split into a numerical and an analytical part. Assuming that $s \neq l$, we get with Eq. (3) a $\tilde{\mathbf{L}}$-matrix with the general structure

$$\tilde{\mathbf{L}}_{sl}(x) = \begin{bmatrix} \ddots & & & & \\ & x\frac{n_s}{n_l} + R_2 & \cdots & -x & \\ & \vdots & \ddots & \vdots & \\ & -x\frac{n_s}{n_l} & \cdots & x + R_1 & \\ & & & & \ddots \end{bmatrix}, \tag{11}$$

where $R_1 = \eta_{ll} + \sum_{j \neq [l,s]} \eta_{sj}$ and $R_2 = \eta_{ss} + \sum_{j \neq [s,l]} \eta_{lj}$. In case of $s = l$ one element of the $\tilde{\mathbf{L}}$-matrix diagonal consists of the entry $x + R_3$ with $R_3 = \sum_{j \neq s} \eta_{sj}$. For both cases $R_{1,2,3}$ does not depend on x and therefore constitutes a numeric residual in the matrix diagonal.

By matrix column/row permutations the $\tilde{\mathbf{L}}$ matrix is transformed into block matrices, where all analytic x-dependent matrix elements are gathered in the $\mathbf{A}$-matrix while all remaining blocks are purely numerical. Then Eq. (1) can be written as

$$\omega_m \begin{bmatrix} \mathbf{A}(x) & \mathbf{B} \\ \mathbf{C} & \mathbf{D} \end{bmatrix} \begin{pmatrix} \mathbf{E}_a \\ \mathbf{E}_b \end{pmatrix} = \begin{pmatrix} \mathbf{P}_a \\ \mathbf{P}_b \end{pmatrix}, \tag{12}$$

and after solving with respect to $\mathbf{E}_a$ we get

$$\mathbf{E}_a = \frac{1}{\omega_m} (\mathbf{A} + \mathbf{B}\mathbf{D}^{-1}\mathbf{C})^{-1}(\mathbf{P}_a - \mathbf{B}\mathbf{D}^{-1}\mathbf{P}_b) = \frac{1}{\omega_m} \bar{\mathbf{A}}^{-1}\bar{\mathbf{P}}, \tag{13}$$

$$\mathbf{E}_b = \frac{1}{\omega_m} \mathbf{D}^{-1}\mathbf{P}_b - \mathbf{D}^{-1}\mathbf{C}\mathbf{E}_a. \tag{14}$$

Only Eq. (13) needs to be solved when the response energy of interest is a component of $\mathbf{E}_a$. Without loss of generality we assume that the response energy of interest is $\tilde{E}_1$ which can always be archived by matrix column and row permutations. Therefore, the $\bar{\mathbf{A}}$-matrix is in general of type (3,3). The initial analytical inversion problem in Eq. (10) of size K is reduced to an analytical matrix inversion of the size 3 and a numerical matrix inversion of size $K - 3$.

With Eq. (13) and with the unit vector $\mathbf{e}_1$ of dimension 3, Eq. (10) becomes

$$G^1_{sl}(\tilde{\boldsymbol{\eta}}, \omega_m) = \frac{\partial}{\partial x}(\mathbf{E}_a \cdot \mathbf{e}_1) = \frac{1}{\omega_m}\frac{\partial}{\partial x}((\bar{\mathbf{A}}^{-1}(x)\bar{\mathbf{P}}) \cdot \mathbf{e}_1) \tag{15}$$

which can easily be solved using the "Sarrus" rule.

3. SEA gradient properties

The question arises as to how the gradient of the reciprocal loss factors, which were eliminated in the parameter space, are effectively computed. With the reciprocal parameter $x_r = \eta_{ls}$ with $x_r = n_s/n_l \cdot x = r \cdot x$ it can be shown in Eq. (11) that $\tilde{\mathbf{L}}_{sl}(x) = \tilde{\mathbf{L}}_{ls}(r \cdot x) = \tilde{\mathbf{L}}_{ls}(x_r)$ holds. Therefore from Eq. (10) we get

$$G^i_{sl}(\tilde{\boldsymbol{\eta}}, \omega_m) = G^i_{ls}(\tilde{\boldsymbol{\eta}}, \omega_m)r \tag{16}$$

and we further analyse that the symmetry

$$G^i_{sl}(\tilde{\boldsymbol{\eta}}, \omega_m)\tilde{\eta}_{sl}(\omega_m) = G^i_{ls}(\tilde{\boldsymbol{\eta}}, \omega_m)\tilde{\eta}_{ls}(\omega_m) \tag{17}$$

holds.

A second question concerns the structure of the gradient with respect to one selected loss factor. We have to distinguish the two cases $x = \tilde{\eta}_{ss}$ is an ILF and $x = \tilde{\eta}_{sl}, s \neq l$ is a CLF. In general the power vector $\bar{\mathbf{P}} = \mathbf{P}_a - \mathbf{B}\mathbf{D}^{-1}\mathbf{P}_b = [\bar{P}_1, \bar{P}_2, \bar{P}_3]^{\mathrm{T}}$ of type (3,1) is fully populated while the matrix $\bar{\mathbf{A}}(x) = \mathbf{A} + \mathbf{B}\mathbf{D}^{-1}\mathbf{C}$ is of the type

$$\bar{\mathbf{A}}(x) = \begin{bmatrix} a_{11} & a_{12} & a_{13} \\ a_{21} & x + a^r_{22} & a_{23} \\ a_{31} & a_{32} & a_{33} \end{bmatrix} \tag{18}$$

when x is an ILF and

$$\bar{\mathbf{A}}(x) = \begin{bmatrix} a_{11} & a_{12} & a_{13} \\ a_{21} & x\dfrac{n_s}{n_l} + a^r_{22} & -x + a^r_{23} \\ a_{31} & -x\dfrac{n_s}{n_l} + a^r_{32} & x + a^r_{33} \end{bmatrix} \tag{19}$$

when x is an CLF. Because of the symmetry of the x parameter in Eqs. (18) and (19) we get for both cases a solution of Eq. (13) which has the linear rational structure

$$\tilde{E}_i(x) = \frac{ax + b}{x + c}, \quad i = 1, 2, 3 \tag{20}$$

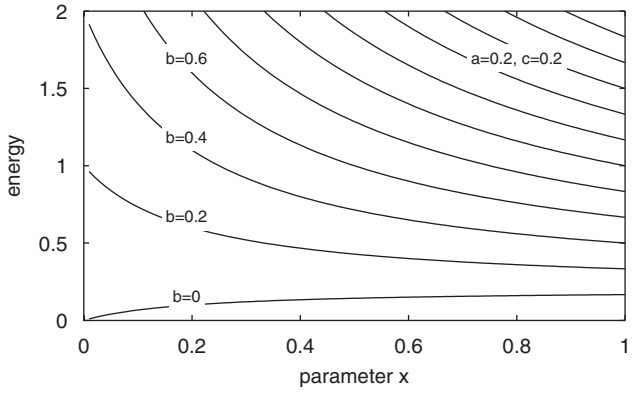

Fig. 1. SEA gradient as a hyperbolic function.

with $a, b, c > 0$ as the total energy itself is a positive function $\forall x > 0$. Eq. (20) represents hyperbolic functions which are depicted in Fig. 1 with fixed parameter $a = c = 0.2$ and varying $0 < b < 0.6$. Gradient (15) results in

$$\frac{\mathrm{d}\tilde{E}_i}{\mathrm{d}x} = \frac{ac - b}{(x + c)^2}. \tag{21}$$

Therefore, the energy is a monotonically increasing function for $ac < b$, a monotonous decreasing function for $b < ac$ or a constant for $b = ac$, see Fig. 1. The diagram also shows that the validity area of a linear approximation at an abscissa point x_0 of the hyperbolae depends very much on a, b, c, x_0.

Out of these results we state that there are no local extrema of the energy function within the parameter space. Hence we expect that an optimisation in the loss factor parameter space would always end up at given parameter margins. On the other hand there is evidence now that the following optimisation procedure yields acceptable results, as the gradient always points in the "right direction".

4. Vibro-acoustic potential analysis

If we assume that the energy of the response subsystem of interest is $\tilde{E}_i$ then the optimisation goal will be

$$\min_{\tilde{\boldsymbol{\eta}}} \{\tilde{E}_i(\omega_m, \tilde{\boldsymbol{\eta}}, \mathbf{P}) | \mathbf{P}(\omega_m) = \mathbf{P}_0, \}. \tag{22}$$

The optimisation takes place for each angular centre frequency ω_m with a fixed setup of power excitation which is defined in $\mathbf{P}_0$. Using a Taylor series of first order $\tilde{E}_i$ can be approximated as

$$\tilde{E}_i(\tilde{\boldsymbol{\eta}}) \approx \tilde{E}_i(\tilde{\boldsymbol{\eta}}^0) + \sum\nolimits_{s,l} \left.\frac{\partial \tilde{E}_i}{\partial \tilde{\eta}_{sl}}\right|_{\tilde{\boldsymbol{\eta}}^0} (\tilde{\eta}_{sl} - \tilde{\eta}^0_{sl}) \tag{23}$$

$$\approx \tilde{E}_i(\tilde{\boldsymbol{\eta}}^0) + \sum\nolimits_{sl} G^i_{sl}(\tilde{\boldsymbol{\eta}}^0)(\tilde{\eta}_{sl} - \tilde{\eta}^0_{sl}). \tag{24}$$

Therefore Eq. (22) becomes

$$\min_{\boldsymbol{\eta}} \{\tilde{E}_i(\tilde{\boldsymbol{\eta}}^0) + \sum_{sl} G^i_{sl}(\tilde{\boldsymbol{\eta}}^0)(\tilde{\eta}_{sl} - \tilde{\eta}^0_{sl}) | \mathbf{P} = \mathbf{P}_0\}. \tag{25}$$

Together with Eq. (15) a common gradient walk optimisation method can be applied in order to solve for an optimum $\tilde{\boldsymbol{\eta}}$ in Eq. (22). In order to optimise within the confidence interval of model (25) the iteration step width $\Delta\tilde{\boldsymbol{\eta}}$ should be bounded. Within each iteration step the gradient needs to be calculated again with respect to $\tilde{\boldsymbol{\eta}} + \Delta\tilde{\boldsymbol{\eta}}$.

Bearing in mind the optimisation procedure of a complete vehicle SEA model, it is necessary to restrict the number of parameters that are changed. Therefore, in practise it is sometimes of more interest to extract a small set of optimisation parameters according to its sensitivities. For each parameter the vibro-acoustic potential and its design target are calculated, which helps quantitatively to evaluate the dominant vibro-acoustic paths within a given frequency range.

4.1. Sensitivity selection

In a first step a small set of the most sensitive SEA parameters must be selected. Because of the difficulty deciding whether it is easier to design an ILF or CLF, both types of sensitivity are regarded separately. It generally holds that $G^i_{\mathrm{ss}} < 0$ as an increase of internal loss of a subsystem always reduces the energy of all subsystems. Therefore, $\Delta\tilde{E}_i$ is minimised when $\tilde{\eta}_{\mathrm{ss}}$ is maximised ($\tilde{\eta}_{\mathrm{ss}} > 0$). For G^i_{sl} experience shows that most of the gradients in a model are positive but not all of them. Hence for a coupling loss factor with $G^i_{sl} > 0$ and because of $\tilde{\eta}_{sl} \geqslant 0$ there exists the lower bound of maximum energy drop at subsystem i

$$\Delta\tilde{E}^{\min}_i = -G^i_{sl}\tilde{\eta}^0_{sl} \tag{26}$$

which can at least be reached by a complete decoupling of the subsystems S_s and S_l.

For all ILF and CLF sensitivities we select the most dominant parameters at angular frequencies ω_{sel} using the following scheme. With

$$\forall s, k_s = \max_{\omega_{\mathrm{sel}}}(|G^i_{\mathrm{ss}}(\omega_{\mathrm{sel}})|) \quad \text{and} \quad \forall s, l, k_{sl} = \max_{\omega_{\mathrm{sel}}}(|G^i_{sl}(\omega_{\mathrm{sel}})\tilde{\eta}^0_{sl}(\omega_{\mathrm{sel}})|) \tag{27}$$

and with the vectors $\mathbf{k}_1 = [\ldots, k_s, \ldots]^{\mathrm{T}}$ and $\mathbf{k}_2 = [\ldots, k_{sl}, \ldots]^{\mathrm{T}}$ we get

$$\mathbf{M}_{\mathrm{ILF}}(n) = \mathrm{sort}_s(\mathbf{k}_1) \quad \text{and} \quad \mathbf{M}_{\mathrm{CLF}}(m) = \mathrm{sort}_{sl}(\mathbf{k}_2). \tag{28}$$

The selection of the first N parameters of the vectors $\mathbf{M}_{\mathrm{ILF}}$ and $\mathbf{M}_{\mathrm{CLF}}$ and the application of the inverse mapping $n \longrightarrow s$ and $m \longrightarrow sl$ which is known from the sorting algorithm yields a set $\mathbf{M}_0 = \{(n, m)\}$ of dominant parameters. For the CLF parameters, Eq. (27) also ensures that the reciprocal parameters need not be taken into consideration because of Eq. (17), and furthermore we ensure that the optimisation potential is greatest because the selection law in Eq. (28) is based on the search of the lower bound of maximum energy drop (26).

4.2. Vibro-acoustic potentials

The vibro-acoustic potential of a single parameter $x = \tilde{\eta}_{sl}$ can be calculated using Eq. (20) when we estimate the three unknown parameters a, b, c. Therefore, three equations are needed where two, $\tilde{E}_i(\tilde{\boldsymbol{\eta}}^0) = E_0$ and the gradient $G^i_{sl}(\tilde{\boldsymbol{\eta}}^0) = G_x$ are already known. A third equation is derived when we, e.g. numerically solve $\tilde{E}_i(\tilde{\boldsymbol{\eta}}^1) = E_1 = 1/\omega_m \tilde{\mathbf{L}}^{-1}(\tilde{\boldsymbol{\eta}}^1)\mathbf{P}$ with $\tilde{\boldsymbol{\eta}}^1 = [\tilde{\eta}^0_{11}, \ldots, \tilde{\eta}_{sl}/2, \ldots, \tilde{\eta}^0_{s+1,l}, \ldots]^{\mathrm{T}}$. The parameters a, b, c can then be estimated by

$$a = \frac{xG_xE_1 + 2E_0E_1 - 2E_0^2}{2E_1 + xG_x - 2E_0}, \tag{29}$$

$$b = -x\frac{E_0E_1 - E_0^2 + xG_xE_1}{2E_1 + xG_x - 2E_0}, \tag{30}$$

$$c = -x\frac{E_1 + xG_x - E_0}{2E_1 + xG_x - 2E_0}. \tag{31}$$

As Eq. (20) is a monotonic function, its minimum within the given parameter margins can be found by

$$E_{x,\min} = \min\left(\left[\lim_{x\to 0+}\frac{ax+b}{x+c}, \lim_{x\to\infty}\frac{ax+b}{x+c}\right]\right) = \min([b/c, a]) \tag{32}$$

which constitutes the vibro-acoustic potential of a parameter $x = \tilde{\eta}_{sl}(\omega_m)$ at a fixed angular frequency ω_m.

4.3. Loss factor design targets

On the other hand a target value x_{tg} which is necessary for communication with a trim material supplier can easily be calculated when a target energy $E_0 > E^{\mathrm{tg}} > E_{x,\min}$ is given. The inversion of Eq. (20) yields

$$x_{\mathrm{tg}} = \frac{E^{\mathrm{tg}}c - b}{a - E^{\mathrm{tg}}} \tag{33}$$

and constitutes the result for a one-dimensional optimisation problem (25) for a fixed frequency. As this optimisation procedure is one dimensional only it easily occurs that $E^{\mathrm{th}} < E_{x,\min}$ which means that the optimisation goal can not be reached. In that case E^{th} should be increased.

Regarding all potentials and target values of the selected parameters in M_0, the resulting design freedom can be used for the definition of an optimum acoustic package within the frequency range, taking into consideration the needs of acoustic trim material suppliers. After application of one measure to the model, one has to bear in mind that the whole procedure should be recalculated in order to get accurate potentials and targets for the remaining parameter set again. On the other hand this step can be omitted when the variation of the parameter is still within the confidence interval of the Taylor approximation in Eq. (24).

For completeness we get from Eq. (10), with ω_m fixed, the gradient with respect to material parameters expressed as $\tilde{\boldsymbol{\eta}} = \mathbf{f}(\boldsymbol{\beta})$, where the vector $\boldsymbol{\beta}$ contains all relevant material parameters using chain rule

$$\nabla_\beta \tilde{E}_i(\boldsymbol{\eta}(\boldsymbol{\beta})) = \nabla_\beta \tilde{\boldsymbol{\eta}}(\boldsymbol{\beta}) \nabla_{\tilde{\eta}} \tilde{E}_i(\tilde{\boldsymbol{\eta}}(\boldsymbol{\beta})), \tag{34}$$

where $\nabla_\beta \boldsymbol{\eta}(\boldsymbol{\beta})$ is a matrix. In general the gradient no longer has a simple hyperbolic structure as each component of $\nabla_\beta \tilde{E}_i(\boldsymbol{\eta}(\boldsymbol{\beta}))$ represents a sum of products between hyperbolae and yet unknown functions which depend on the particular material laws.

At MAGNA STEYR a MATLAB toolbox was developed which calculates the SEA sensitivity in Eq. (15) the vibro-acoustic potentials (32) and design targets (33) of a given set of loss factors. The loss factor set is defined by a column and row position (s, l) within the **L**-matrix. MATLAB functions also support the setup of the parameter vector set with additional filtering options, e.g. when only coupling between flexure and shear wave types is of interest. Last but not least the AutoSEA MATLAB-API from ESI Group is used in order to retrieve the **L**-matrix from a given AutoSEA model efficiently.

5. Validation example

For validation purpose we have selected a model part consisting of 8 subsystems from the AutoSEA demo Model "Airplane.va2" which is part of the AutoSEA 2004 distribution, see Fig. 2. All wave types are switched on. We applied a constant flexural excitation of 1 W within the bandwidth at subsystem "Fuselage 3 Top Right" and defined the cavity "SPL_Seats_3" as the response subsystem.

Using Eq. (15), the gradients of all 20 ILFs and 136 CLFs of the model are computed within the frequency band $500\,\text{Hz} \leqslant f_m \leqslant 10\,\text{kHz}$. The sensitivity analysis revealed that the most dominant ILF parameter $\eta_{20,20}$ corresponds with the response subsystem and that the most dominant CLF parameter $\eta_{15,19}$ corresponds with the area coupling "Storage Trim 3 Right" flexure to "Trim Air Gap 3 Right" which is a cavity subsystem, see

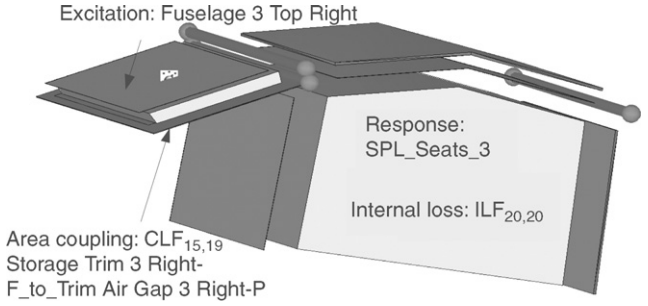

Fig. 2. Validation model and the most sensitive ILF ($\eta_{20,20}$) and CLF ($\eta_{15,19}$) parameters.

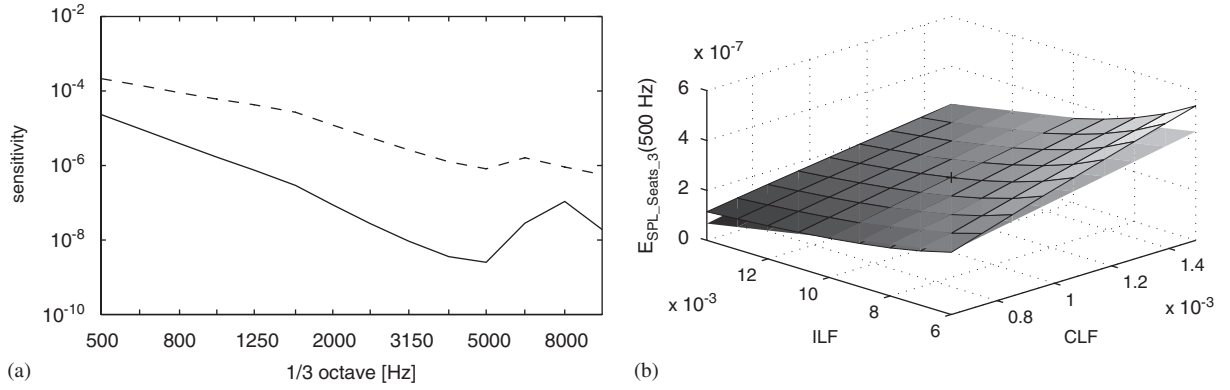

Fig. 3. (a) Sensitivities of the selected CLF (dotted line) and ILF (solid line) parameters. (b) Variation energy of the response subsystem due to a change of the selected parameters. The gradient is displayed as the flat plane.

Fig. 3(a). The diagram shows that within the whole frequency range the CLF has the greatest influence on the energy. Bearing in mind the different signs of the sensitivities, the energy is reduced by increasing the ILF and decreasing the CLF.

Regarding the 2-dimensional parameter space $\{\eta_{20,20}, \eta_{15,19}\}$ a comparison between the numerical model (hyperbolic surface) which was computed using AutoSEA and the approximate model (24) is shown in Fig. 3(b). The parameters are varied between $\pm 40\%$. The diagram confirms the conclusion from Section 3 that there should not exist a local extrema. Furthermore, the diagram shows a good correlation between the "real" model from AutoSEA and the approximate model.

6. Engine noise optimisation

Based on a coupé trimmed body (TB) SEA model, see Fig. 4, whose loss factors are derived by the "power injection method" (PIM) measurement, see Refs. [3,11–14], we apply the proposed vibro-acoustic potential analysis to the model. The use of PIM also results in SEA parameters for structural coupling, which is not the case when loss factors are derived from transmission loss and absorption measurements. The rather coarse AutoSEA model consists of 82 subsystems (33 flat-, 38 singly curved-, 1 doubly curved plate and 10 cavities). As an example, a power input configuration was developed by wide open throttle measurements on a dynamometer rig at 4000 rev/min constant speed. The design and validation of the model and the SEA source measurements took place in cooperation with the Acoustic Competence Centre in Graz.

For the dynamometer rig measurements the engine noise was considered to excite the engine bay by air-borne and the front longitudinal members by structural excitation. The contribution of rolling noise was omitted due to the strong engine noise presence. The exhaust system was assembled beside the car so that structural excitations where reduced. The air-borne fractions were reduced by additional damping measures. The measurement results in average velocities of the front longitudinal members and an average pressure level of the engine bay. After application of these vectors to a SEA model as constraints with correct masses and volumes for the constrained subsystem we could retrieve the effective input power vectors from AutoSEA, see Fig. 5(a). While the dotted line shows the air-borne power input which is applied at the engine bay, the solid line shows the

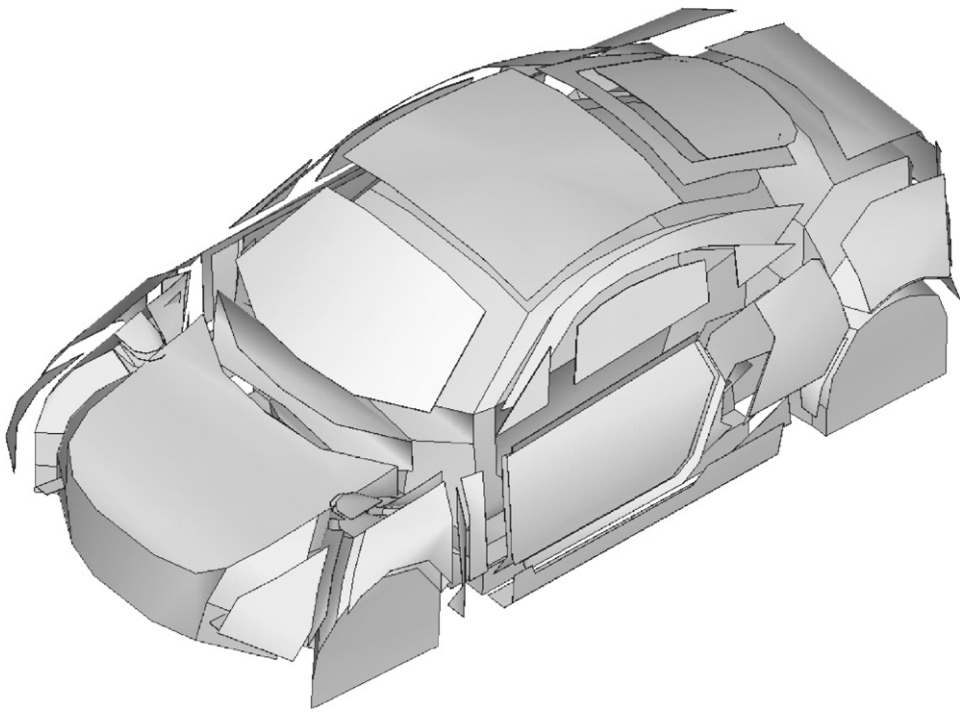

Fig. 4. SEA model of a coupé trimmed body consisting of 82 subsystems.

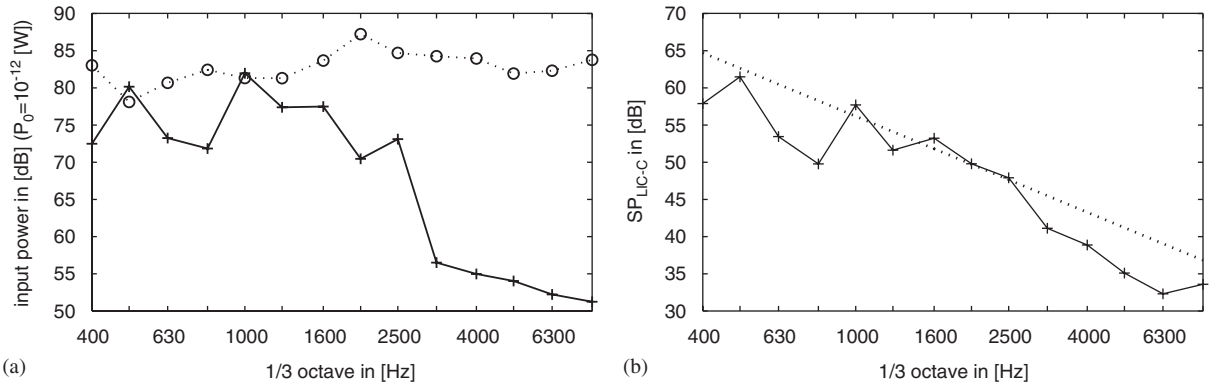

Fig. 5. (a) Structural (solid line) and acoustic (dotted line) effective input powers related to engine noise. (b) Simulated in-cabin SPL according to the input power configuration. A target SPL (dotted line) is depicted for further investigations.

structure borne excitation which is applied two times (left and right longitudinal member) in the model. For frequencies above 1.6 kHz the air-borne excitation dominates the structural excitation (graph + 3 dB) by more than 10 dB. In the lower-frequency range there are two structural power peaks at 500 Hz and at 1 kHz which surpass the air-borne excitation levels. The passenger compartment was chosen as the response subsystem. The simulated response in-cabin SPL can be seen in Fig. 5(b). As an example the target in-cabin SPL was chosen according to the thick dotted line in the diagram which is surpassed by the simulated SPL for the angular frequencies $f_{\mathrm{sel}} = [1, 1.6, 2, 2.5]^{\mathrm{T}}$ kHz.

In total the model consists of 174 ILF and 1555 CLF parameters. There are more ILFs than subsystems as the structural subsystems which have not been treated according to PIM are mathematically modelled as three individual subsystems each for one of the wave types "flexure", "extension" and "shear". The selection of the first four dominant loss factors according to Eqs. (27, 28) with respect to f_{sel} yields the following ranking for ILFs and CLFs:

Ranking	ILFs	CLFs
1	IC-C	IC-C to DB-F
2	UF-F	IC-C to FW-F
3	DB-F	DB-F to FW-F
4	FWA-F	LM-F to FW-F

The abbreviations: "in-cabin cavity (IC-C)", "under-floor cavity (UF-C)", "dashboard flexure wave type (DB-F)", "front wheel arch flexure wave type (FWA-F)" and "longitudinal member flexure wave type (LM-F)" have been used. The sensitivities according to Eq. (15) are depicted in Fig. 6. The analysis reveals that sensitivities of CLFs in diagram (b) dominate the in-cabin SPL by a factor 100 more then the sensitivities of the ILFs in diagram (a). Furthermore, a comparison between the ranking table and the CLF sensitivity values in the diagram shows a sequencing difference which shows that the search in Eq. (28) yields to different results when compared with a search of a maximal sensitivity alone.

For all selected parameters the vibro-acoustic potentials are displayed in Fig. 7. Diagram (a) shows the ILF potentials. The curve for "IC-C" is missing as its curve is below −100 dB which means that for a theoretical damping $\eta_{\mathrm{IC-C}} \to \infty$ the in-cabin SPL will tend to zero. Therefore, an increase of in-cabin damping would be most effective. Of course the same would hold for the excitation subsystem in the case of a single source configuration. On the other hand the diagram shows potentials from 0 to 4 dB which suggest additional structural damping for the dashboard and the front wheel housings (left and right structural excitation subsystems). The suggested damping increase of the under-floor cavity is hard to influence and therefore omitted. The investigation of diagram (b) reveals potentials between 1 and 2 dB when reducing the coupling "IC-C to DB-F" and "IC-C to FW-F". The potential is below 1 dB for the two remaining structural couplings "DB-F to FW-F" and "LM-F to FW-F".

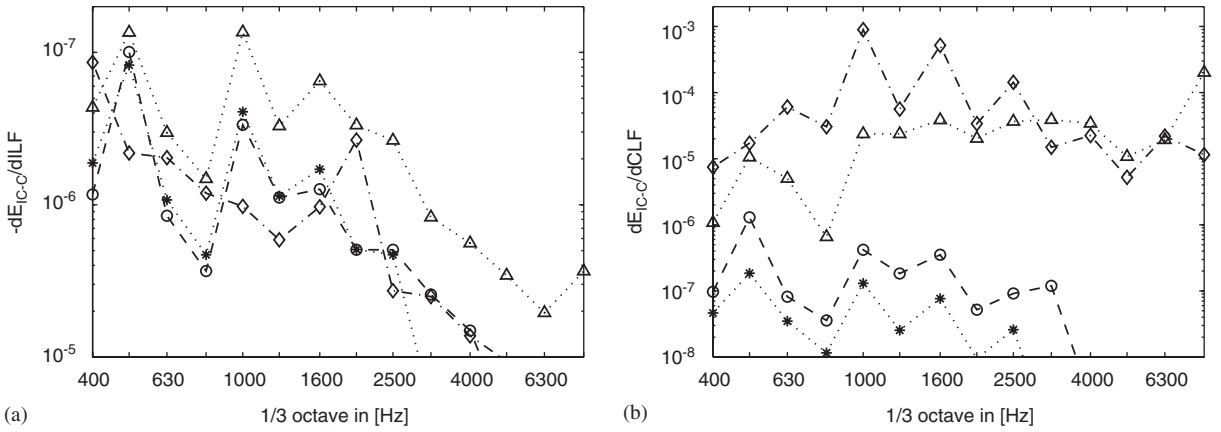

Fig. 6. Dominant sensitivities for engine excitation. (a) ILF sensitivities: ··△··, IC-C; ·–◇–·, UF-C; – ◦ –, DB-F; ··⋆··, FWA-F. (b) CLF: ··△··, IC-C to DB-F; ·–◇–·, IC-C to FW-F; – ◦ –, DB-F to FW-F; ··⋆··, LM-F to FW-F.

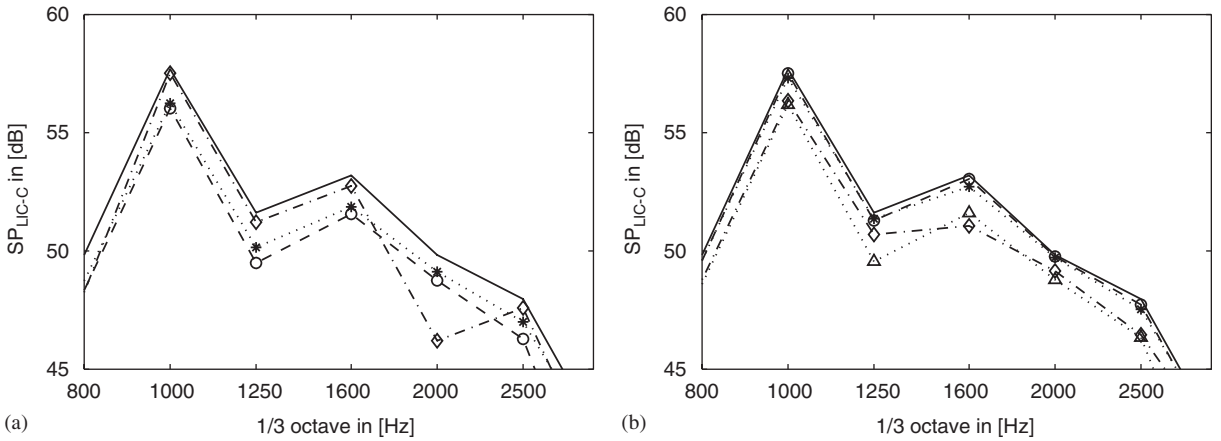

Fig. 7. Potential decrease of in-cabin SPL of the selected parameters. (a) shows ILF potentials: —, baseline; ··△··, IC-C; ·–◇–·, UF-C; – ◦ –, DB-F; ··⋆··, FWA-F. (b) CLF potentials: —, baseline; ··△··, IC-C to DB-F; ·–◇–·, IC-C to FW-F; – ◦ –, DB-F to FW-F; ··⋆··, LM-F to FW-F.

The design target SPL in Fig. 5(b) can be related to a threshold energy $E^{\mathrm{th}} = V/(\rho c^2)P_a^2$ with $V_{\mathrm{IC-C}} = 2.527m^3$. Therefore, we get the target energy

$$E^{\mathrm{tg}}(\omega_m) = \begin{cases} E_0(\omega_m) & \forall\ E_0(\omega_m) <= E^{\mathrm{th}}(\omega_m), \\ E^{\mathrm{th}}(\omega_m) & \forall\ E_0(\omega_m) > E^{\mathrm{th}}(\omega_m). \end{cases} \tag{35}$$

With Eq. (33) the loss factor targets can be computed. The results are displayed in Fig. 8. For the design of damping measures, shown in the diagrams (a–e) it is suggested to slightly increase the damping of "IC-C" or otherwise to increase the structural damping of "DB-F". As already mentioned there are no meaningful measures to increase the underfloor damping. And last but not least the target damping curve for flexural damping of "FWA-F" only shows one meaningful target value at 2.5 kHz. All other values are missing because of $E^{\mathrm{tg}} < E_{x,\min}$ or are inadmissible as they are too high. On the other hand the targets can also be reached by a decrease of the coupling "IR-C to DB-F" except at 1 kHz, see diagrams (e–h). The remaining three target CLFs show that they turn negative (no value displayed) for one or more frequencies. So the target cannot be reached by a single CLF-decreasing measure.

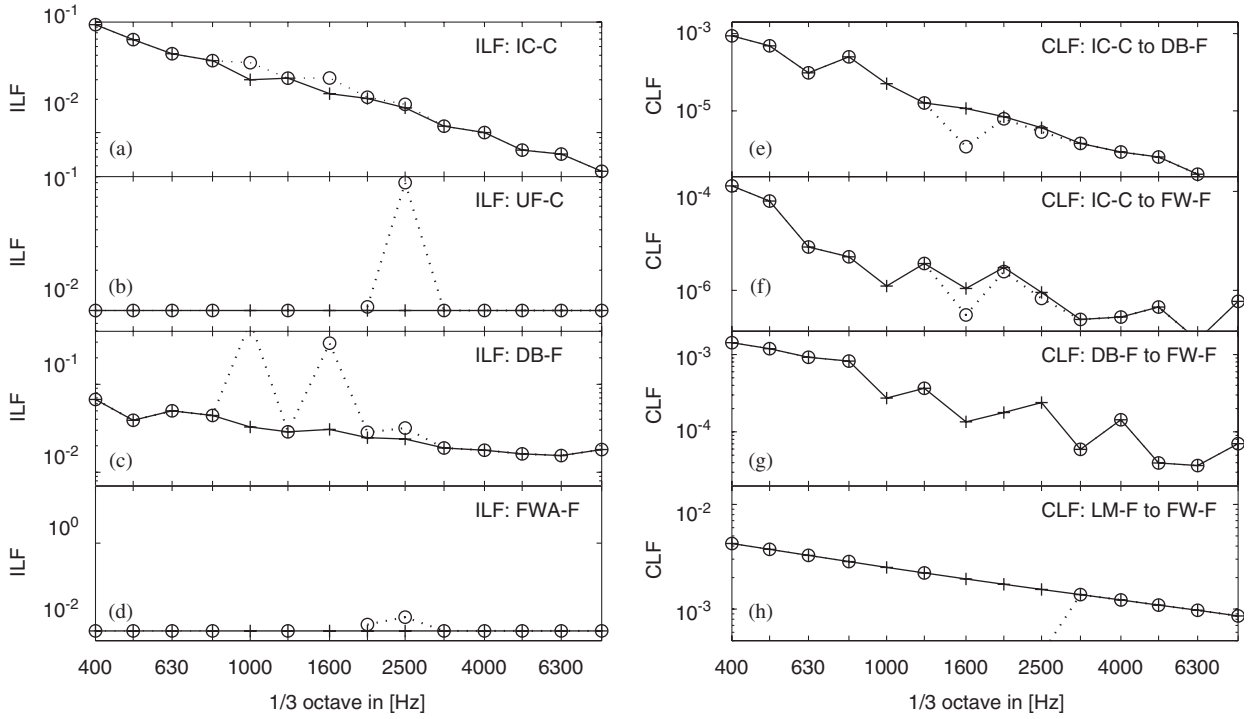

Fig. 8. Design targets for the selected parameters: (a–d) ILF design targets; and (e–h) CLF design targets. The solid graphs represent the origin loss factor values while the dotted lines indicate the design targets. A missing target value indicates that the design target cannot be fulfilled.

Despite the much higher sensitivity of the CLFs compared with the ILFs in the given example, it can be seen that an optimisation using CLFs is more difficult.

In order to design the acoustic damping of "IC-C" in general only the absorption of the surface of the cavity can be influenced, being related to the ILF according to

$$\alpha_m(\omega_m) = \tilde{\eta}_{ss}(\omega_m)\frac{4V\omega_m}{Ac_0}, \tag{36}$$

where V is the volume, A the surface area and c_0 the phase speed of the fluid air. The overall absorption taking into account an inhomogeneous surface is defined as

$$\alpha_m(\omega_m) = \sum_{i=1}^{n} \alpha_i(\omega_m)A_i / \sum_{i=1}^{n} A_i. \tag{37}$$

This procedure can be understood as a separate optimisation step which is in general carried out in cooperation with a material supplier as it strongly depends on material parameters and trim production process parameters.

In order to consider the results from the ILF/CLF potential analysis it is suggested to use the design targets in Fig. 8 and the analysis results from Eqs. (36) and (37) as an interface between a system supplier like MAGNA STEYR and a trim material supplier. This allows a more specific determination of trim optimisation goals and also a detailed evaluation of the vibro-acoustic performance of a given trim package, which takes into consideration that dominant vibro-acoustic paths are changing within the frequency range. When using a set M_0 of design parameters the method also provides enough freedom for a cost-efficient trim part optimisation as there are still several possibilities regarding how to reach the acoustic targets.

7. Conclusion

The analytical analysis of the properties of the gradient of the energy with respect to the SEA loss factors shows the absence of local extrema in the loss factor space. Therefore, we suggest the application of the vibro-acoustic potential analysis introduced here as a simple optimisation procedure that reveals insulation and damping measures for both air-borne and structural paths.

Here it has been shown that SPL targets given by an OEM can be transformed into design targets for material suppliers that still provide enough freedom for cost efficient trim part optimisation. This suggested interface seems well suited to an optimisation process in which the complete vehicle and trim material are not developed within the same company.

Acknowledgement

The authors wish to thank Mr. G. Müller and Mr. P. Cox from MAGNA STEYR Fahrzeugtechnik for their great efforts which helped to improve the nomenclature and grammar of our manuscript significantly.

References

[1] R. Lyon, G. Maidanik, Power flow between linearly coupled oscillators, *The Journal of the Acoustical Society of America* 34 (1962) 623–639.
[2] P. Smith Jr., Response and radiation of structural modes excited by sound, *The Journal of the Acoustical Society of America* 34 (1962) 640–647.
[3] R. Lyon, R. DeJong, *Theory and Application of Statistical Energy Analysis*, second ed., Butterworth-Heinemann, London, 1995.
[4] S. Korte, Optimization of a car floor damping based on a complete AutoSEA car model using a genetic optimization algorithm, *Proceedings of the Second Vibro-Acoustic User Conference*, Vibro-Acoustic Sciences, Inc., Paris, France, 2004.
[5] M. Dinsmore, R. Unglenieks, Acoustical optimization using quasi-Monte Carlo methods and SEA modeling, *Proceedings of the 2005 Noise and Vibration Conference*, Society of Automotive Engineers (SAE), Traverse City, USA, 2005.
[6] J. Rodriguez-Ahlquist, J.-C. Bonnet, Efficient sound package design using statistical energy analysis with optimisation through genetic algorithm, *Proceedings of Joint Meeting of the German and the French Acoustical Societies*, Fortschritte der Akustik, CFA/DEGA e.V., Strasbourg, France, 2004, pp. 9–10.
[7] H. He, J. Pan, A. Luebke, From complex vehicle requirements to component design—a case study of sound package early development using SEA genetic optimization and system engineering, *Proceedings of the 2005 Noise and Vibration Conference*, Society of Automotive Engineers (SAE), Traverse City, USA, 2005.
[8] K. Misaji, H. Tada, N. Baldanzini, H. Pätzold, M. Mantovani, Optimal design of a sound package component within the Rieter automotive VECTOR system, *Proceedings of the Rieter Automotive Systems*, Lucerne, Switzerland, 2003.
[9] E. Sarradj, Bestimmung v. Sensitivitäten mit der Statistischen Energieanalyse, *Proceedings of the 22nd Annual Conference for Acoustics*, Fortschritte der Akustik, DEGA e.V., Bonn, Germany, 1996, pp. 204–205.
[10] N. Lalor, G. Stimpson, FEM + SEA + OPTIMISATION = LOW NOISE, *Second International Conference, Vehicle Comfort: Ergonomic, Vibrational, Noise and Thermal Aspects*, Technical Papers, Vol. 1, Bologna, Italy, 1992, pp. 134–160.
[11] D. Bies, S. Hamid, In Situ determination of loss and coupling loss factors by the power injection method, *Journal of Sound and Vibration* 70 (2) (1980) 187–204.
[12] M. Heckl, M. Lewit, Statistical energy analysis as a tool for quantifying sound and vibration transmission paths, in: A. Kaene, W. Price (Eds.), *Statistical Energy Analysis*, Cambridge University Press, Cambridge, 1994, pp. 19–34.
[13] N. Lalor, Practical considerations for the measurement of internal and coupling loss factors on complex structures, Technical Report 182, Institute of Sound and Vibration Research, 1990.
[14] K.D. Langhe, P. Sas, Statistical analysis of the power injection method, *The Journal of the Acoustical Society of America* 100 (1996) 294–303.